Probabilistic modeling of eruptive activity at Etna volcano using InSAR surface displacements and ATSR thermal radiance

M. R. Patrick,[1,2] L. N. Frazer,[3] and B. A. Brooks[1]

Received 5 June 2006; revised 27 July 2006; accepted 1 August 2006; published 28 September 2006.

[1] Satellite monitoring offers a powerful means to regularly characterize the mechanical and thermal states of active volcanoes. Satellite-measured surface inflation and radiant heat flux reflect the pressurization and discharge, respectively, of a magmatic system, suggesting that studying these parameters together may help in better understanding future eruptive activity. We incorporate InSAR surface displacement data and ATSR thermal radiance data into a probabilistic model for activity at Etna volcano in 1996–2000, when surface deformation and thermal radiance appeared to be related in a periodic fashion. The probabilistic approach addresses both the magnitude and timing of eruptive events, based upon a simple physical model of eruptions as renewal processes. We anticipate that this approach could serve as a framework for probabilistic assessment in eruption scenarios with persistent activity and multiple monitoring datastreams. **Citation:** Patrick, M. R., L. N. Frazer, and B. A. Brooks (2006), Probabilistic modeling of eruptive activity at Etna volcano using InSAR surface displacements and ATSR thermal radiance, *Geophys. Res. Lett.*, *33*, L18312, doi:10.1029/2006GL026983.

1. Introduction

[2] Space-based volcano monitoring has greatly advanced our understanding of the physical processes governing how, when, and where volcanoes erupt. In particular, independently acquired geodetic and thermal radiance data have proven indispensable in support of daily global monitoring and in specific eruption crises [*Francis and Rothery*, 2000; *Dzurisin*, 2003]. Although the two datasets are complementary in temporal and physical terms – surface inflation indicates shallow emplacement of magma prior to an eruption, while thermal radiance results from the expulsion of that magma during an eruption – little attention has been focused on their joint analysis.

[3] Probabilistic modeling offers a means to combine insights from multiple datatypes, such as deformation and radiance, to characterize the chance of upcoming eruptive activity. A common approach for modeling eruption repose periods relies upon the concept of a renewal process - in a volcanic context this might be the repeated filling, pressurization and eruption of magma in a shallow reservoir. Previous probabilistic modeling of eruptions has focused primarily on the timing of major eruptions [*Voight*, 1988; *Connor and Hill*, 1995; *Ho*, 1996; *Bebbington and Lai*, 1996; *Jones et al.*, 1999; *Cronin et al.*, 2001; *De la Cruz-Reyna and Carrasco-Núñez*, 2002; *Connor et al.*, 2003]. Alternatively, persistently active volcanoes may exhibit minor to moderate eruptive activity in the intervening periods between major eruptive events, and these smaller scale eruptions can affect the magma budget in the reservoir and the timescale of the renewal process, or they may present hazards of their own.

[4] Here, we merge information from surface deformation (InSAR, interferometric synthetic aperture radar) and thermal radiance observations (ATSR, along track scanning radiometer) using a simple probabilistic model that is based upon the renewal concept for eruption recurrence. The renewal model is incorporated into a probability distribution function that characterizes the volume of erupted material, and we apply this probabilistic model to Etna volcano during its 1996–2000 summit activity phase.

2. Mt. Etna Activity and Data Collection

[5] Mt. Etna, in southern Italy, is a complex stratovolcano that has exhibited nearly continuous eruptive activity throughout recorded time, consisting of frequent small-scale explosive activity at the summit and less frequent large-scale effusive eruptions from the flanks. Since the mid 20th century Etna has experienced a significant increase in magma output rate compared to the preceding three hundred years [*Behncke and Neri*, 2003]. Following the voluminous 1991–1993 flank eruption, a two-year period of relative quiescence ensued, followed by nearly continuous summit activity during 1995–2001. This phase of summit activity was notably vigorous, with all four summit craters involved, and produced more than 120 explosive episodes as well as several lava flows [*Behncke and Neri*, 2003]. In July–August 2001 a major flank eruption occurred, followed by another major flank eruption from Oct. 2002 to Jan. 2003, and finally the most recent flank eruption from Sept. 2004 to Jan. 2005 [*Smithsonian Institution*, 2005].

[6] For deformation, we use data from *Lundgren et al.* [2004; their Figure 4a], who mapped Etna surface displacements from InSAR data using the short baseline approach [*Berardino et al.*, 2002] applied to a dataset of over 400 interferograms. Figure 1 shows the motion of the area of maximum inflation/deflation measured on the volcano at a given time, relative to the surface position immediately following the 1991–1993 eruptive phase. The period from 1996–2001 was characterized by deformation fluctuations with a period of ~1 year and amplitude of approximately

[1]Hawaii Institute of Geophysics and Planetology, School of Ocean and Earth Science and Technology, University of Hawaii Manoa, Honolulu, Hawaii, USA.
[2]Now at Department of Geological and Mining Engineering and Sciences, Michigan Technological University, Houghton, Michigan, USA.
[3]Department of Geology and Geophysics, School of Ocean and Earth Science and Technology, University of Hawaii Manoa, Honolulu, Hawaii, USA.

0094-8276/06/2006GL026983$05.00

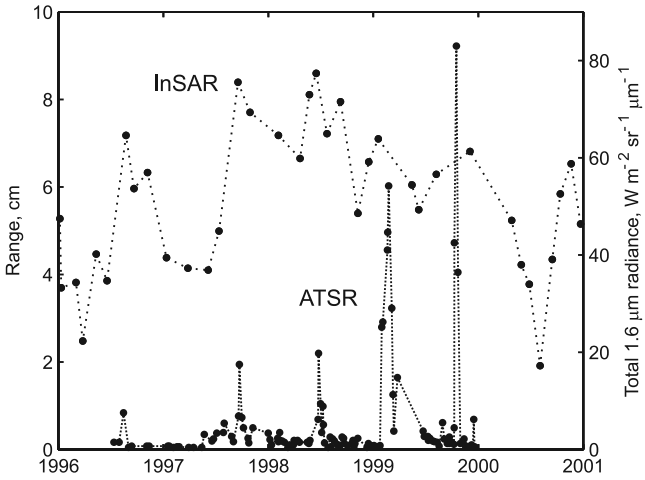

Figure 1. InSAR maximum surface displacement and ATSR radiance for Etna volcano. Adapted from *Lundgren et al.* [2004] and *Rothery et al.* [2001]. Five joint oscillations can be observed, with a mean period of 0.8 years.

3 cm until mid-1998 when oscillations become less pronounced.

[7] In addition to deformation, we use a satellite-derived proxy for radiant heat flux, originating from ATSR-2 data presented in *Rothery et al.* [2001; their Figure 6]. The ATSR sensor acquires in both visible and infrared wavelengths at 1 km pixel size, with a three day repeat period for nighttime scenes. *Rothery et al.* [2001] used the summed nighttime 1.6 micron-channel radiance in Etna images spanning 1996–2000, limiting the summation to those pixels comprising the volcanic thermal anomaly. The 1.6 micron channel is highly sensitive to active, exposed lava due to its proximity to the peak emission wavelength of surfaces at ~1000 °C. Likewise, the 1.6 micron channel is insensitive to warm areas – that emit at longer wavelengths - such as fumarolically active crater interiors. The 1.6 micron summation technique therefore offers a proxy for the total radiant heat outflux from surface magmatic activity.

[8] At Etna the 1995–2000 period was characterized by several discrete peaks in radiance superimposed on much lower levels of apparent background summit activity (Figure 1). *Rothery et al.* [2001] link these discrete peaks to notable events including 1) Aug. 1996: a small lava flow, NE crater, 2) Sept. 1997: ponded lava in Bocca Nuova, 3) June 1998: Bocca Nuova explosions, 4) Feb.–Mar. 1999: SE crater lava flows and 5) Oct 1999: Bocca Nuova lava flows. Due to the three day sampling period some events were missed, including the large fire fountaining episodes in July 1998 and September 1999 from Voragine crater. Both occur relatively close in time to the detected events, however, and therefore do not greatly change the observed periodicity. Most importantly, we note that the peaks and troughs in radiance are generally coincident with those of surface deformation, suggesting they may be causally related.

3. Probabilistic Modeling With Application to Etna

[9] We base our probabilistic approach on a simple physical model of eruptions as renewal processes modulated by steady recharge into a shallow magma reservoir of constant total capacity. The amount of magma within the reservoir at a given time will control the internal pressure and thus the eruptive potential. Internal pressure and eruptive volume, in turn, will control the level of surface deformation and radiant heat flux, respectively. The renewal model is a common conceptual explanation for eruptive periodicity [e.g., *Mann et al.*, 2002; *Dvorak and Dzurisin*, 1993] and is generally consistent with the results of *La Delfa et al.* [2001], which indicated that the small shallow reservoir at Etna was gradually invaded by more primitive magma from depth throughout 1995–2000.

[10] We aim to estimate $P(Q_\Delta(t))$, the probability density function (PDF) of $Q_\Delta(t)$. $Q_\Delta(t)$ is the radiance integrated over some time interval, Δ, and Q_Δ is used here as a rough proxy for erupted volume and overall activity level, which are the variables of primary interest. Previous studies have shown an empirical relation between total radiant heat flux and effusion rate [*Harris et al.*, 1997; *Wright et al.*, 2001], and here we use the 1.6 micron radiance as a proxy for total radiant heat flux levels. In this case:

$$Q_\Delta(t) = \int_t^{t+\Delta} Q(t')dt' \tag{1}$$

where t' is a dummy variable. Our proposed form for $P(Q_\Delta(t))$ is the exponential distribution, which is supported by the exponential nature of the radiance distribution (not shown). The probability distribution thus considers the probability of low values of Q_Δ to naturally tend to be highest at any given time, with the probability declining exponentially with higher values of Q_Δ:

$$P(Q_\Delta(t)) = \lambda \exp[-\lambda Q_\Delta(t)] \tag{2}$$

The rate of this decline is determined by λ, the rate parameter, which is formed by reconciling our renewal model with the actual monitoring data. The individual monitoring datasets, radiant heat flux and deformation, are incorporated into the rate parameter using predictor variables, $x(t)$ and $y(t)$, respectively. Thus, the general objective is to forecast the erupted volume (represented by the radiance proxy Q_Δ), while using radiance and deformation to jointly parameterize the probabilistic model. A summation approach is used to combine the predictor variables:

$$P(Q_\Delta(t)) = (ax(t) + by(t)) \exp[-(ax(t) + by(t))Q_\Delta(t)] \tag{3}$$

where coefficients a and b are weighting factors for the respective predictor variables. Predictor variables are created by the convolution of a window filter with the monitoring data. In the case of radiant heat flux, the predictor variable $x(t)$ is:

$$x(t) = (W_Q * Q)(t) = \int_{-\infty}^{0} W_Q(t - t')Q(t')dt' \tag{4}$$

where W_Q is the radiance window filter and Q is the measured radiant heat flux.

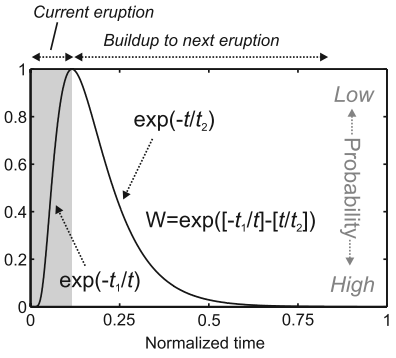

Figure 2. Normalized window filter. Predictor variables and resulting rate parameter are formed by the convolution of this filter with each monitoring dataset. Note the inverse relation between the window filter and resultant probability, due to the negative exponential in equation (2).

[11] The window filter reflects the temporal renewal model for eruptive activity. The probability of the next eruption (producing a volume proxy of Q_Δ) occurring at a given time will decrease as the current eruption discharges magma from the reservoir. This is followed by an increase in the probability as the magma reservoir subsequently recharges. A compound exponential distribution characterizing this model is therefore chosen for the radiance window filter (Figure 2):

$$W_Q(t) = n \exp\left[\frac{-t_{Q1}}{t} - \frac{t}{t_{Q2}}\right] H(t) \tag{5}$$

where n is a constant that ensures the integral of $W_Q(t)$ is unity, t_{Q1} and t_{Q2} control the waxing and waning timescales of the filter, respectively, (Figure 2), and $H(t)$ is a Heaviside function which sets the filter to zero for $t < 0$. Note the inverse relation between the window filter and resultant probability due to the negative exponential in equation (2); Figure 2 indicates the lowest probability of the next large eruption (i.e. at the apex of W_Q) occurs when the magma in the reservoir has been exhausted by the current eruption.

[12] For surface deformation, the predictor variable convolution is:

$$y(t) = (W_D * D)(t) \tag{6}$$

where W_D is identical in form to W_Q, but formed by t_{D1} and t_{D2}. Each predictor variable is normalized such that the sum of its squared values equals unity. The values for t_{Q1}, t_{Q2}, t_{D1}, t_{D2}, a and b are found by maximizing the likelihood function (L) through a minimization of the cost function (E):

$$L = \prod_t (ax(t) + by(t)) \exp[-(ax(t) + by(t))Q_\Delta(t)] \tag{7}$$

$$E = -2\ln(L) = -2\sum_t \{\ln(ax(t) + by(t)) - (ax(t) + by(t))Q_\Delta(t)\} \tag{8}$$

[13] The window filter outlined above was found to be most effective when convolved with data consisting of discrete peaks on a zero background. While the radiance data meet these criteria, the deformation data required subtraction of the original signal from a smoothed version. A short duration causal (i.e. looking back in time) smoothing window (3 month) was found to isolate the inflation peaks best. The difference between the original and smoothed deformation data was then thresholded to leave the inflation peaks, on a zero-value background. Furthermore, we found that this approach was not applicable to radiance events of dramatically different peak amplitudes, due to the constant reservoir capacity assumed in our conceptual model, and therefore the radiance data were normalized by dividing by the maximum value in a causal window with a 1.1 year span (the longest repose period) to remove the long-term rise in values. Note that smoothing must be causal for the model to have predictive value.

[14] With a bootstrap-like approach we used the entire dataset (a total of five oscillations) to find optimal values for t_{Q1}, t_{Q2}, t_{D1}, t_{D2}. The bootstrap-like method consisted of separating the five events at their midpoints and randomly appending them into a simulated sequence of 100 events. The optimization was performed using a recursive grid search to minimize the cost function (equation (8)) over the parameter space for this 100-event sequence. Separate optimizations were performed for each predictor variable to establish the respective t_1 and t_2 which best fit the data, followed by a joint optimization for coefficients a and b. These optimized values were held fixed and used to apply equations (3)–(6) to the entire five-event dataset. This retrospective approach was deemed preferable to optimizing the model parameters with, say, just three events and applying it in a simulated predictive sense to the remaining two.

[15] Figure 3 shows the transformed data (Figure 3a), the predictor variable convolution (Figure 3b), the optimized combination of the individual weighted predictor variables, or λ (Figure 3c), Q_Δ (Figure 3d), the expected Q_Δ (Figure 3e) and the resulting probability density function, $P(Q_\Delta)$ (Figure 3f) throughout 1996–2000. The shape of λ in Figure 3c shows that the deformation predictor variable was weighted much more heavily than that of radiance; the ratio of a to b was 1:7. This ratio tells us that past deformation data was a good predictor of future radiance data but that past radiance data also had predictive value. Because both radiance and deformation are smoothed by the window filter the original difference in the smoothness of the data plays no part in this weighting difference. An arbitrary value of one month was chosen for Δ. The PDF results show that the probability of lower values of Q_Δ is always higher, reflecting our exponential PDF. Additionally, probability ramps up for higher Q_Δ values before each major event, followed by a sharp decline following each event. Optimized values (shown as mean ±st.dev.) for t_{Q1}, t_{Q2}, t_{D1}, t_{D2}, a and b were 0.28(±0.02), 0.18(±0.01), 0.70(±0.02), 0.14(±0.01), $2.9 \times 10^4(\pm 3 \times 10^3)$, $1.99 \times 10^5(\pm 6 \times 10^3)$, respectively, determined by ten iterations of our bootstrap-like optimization approach.

4. Discussion and Conclusions

[16] The above application of the model relied on a retrospective approach due to the few oscillations

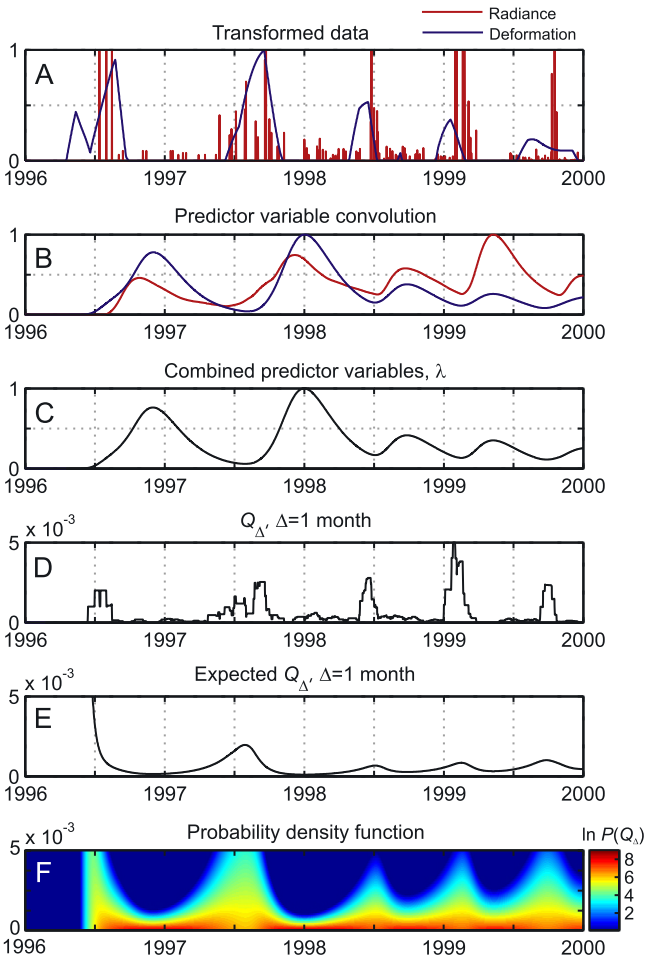

Figure 3. Input data and results for the probabilistic model. (a) The transformed and normalized version of the original radiance and deformation data in Figure 1. (b) Normalized respective predictor variables formed from equations (4) and (6). (c) Normalized combined predictor variables, or λ. (d) Q_Δ, or Q integrated over time interval Δ (1 month here). (e) Expected Q_Δ, calculated by integrating the PDF at a given time. (f) The final PDF, showing hot colors for higher probabilities of a given Q_Δ (y-axis) at a given time (x-axis).

observed - as opposed to applying the model in a truly predictive way - which we deem a reasonable limitation in this proof-of-concept exercise. The results (Figure 3f) show ramping of high probabilities before each major event that may have been useful precursors, indicating that the model can provide an interpretable result and a potentially useful tool in monitoring scenarios. It could be argued that a simple statistical analysis of the repose periods between major events would also provide a serviceable forecasting tool, however, the strength of the approach we outline here is that both the timing and volume of events can be quantified in a probabilistic sense. An inherent limitation of the model relates to the assumption of constant magma renewal and constant reservoir capacity, as evidenced by a discrepancy with the observational data. Figure 1 shows the magnitude of the radiance events increasing dramatically with time, pointing to increases in either magma flux or reservoir, or both. Thus, a process was in place that we could not account for, requiring normalization of the radiance data.

[17] With these limitations in mind, the approach we outline offers several new tools that should be useful for future probabilistic analysis of volcanoes. First, the model jointly considers probability of the timing of activity as well as the erupted volume. The temporal probability is parameterized by the window filter, and volume probability is parameterized by the exponential probability distribution. This differs from existing studies which address probabilistic modeling using a renewal framework in a strictly temporal sense, in essence assuming similarity in the scale of all eruptive events [e.g., *Ho*, 1996; *Bebbington and Lai*, 1996; *Jones et al.*, 1999]. Second, we use multiple disparate remotely-sensed datasets to build the PDF. In volcano monitoring, several data streams are typically collected with each offering potential insight on the underlying physical process driving eruption timing. For instance, both seismicity and surface deformation can reflect gradual invasion of new magma into shallow levels [*Tilling et al.*, 1987] or growing pressurization inside a silicic dome [*Voight et al.*, 1998]. Merging information from multiple data sources increases the potential value of a PDF. Finally, we have also explicitly considered finite eruption duration. Although the eruption timescale is typically much shorter than the replenishment timescale, it is nonetheless simple to account for in this approach.

[18] This study offers a framework for considering the timing and magnitude of eruptive events in a probabilistic sense. For Etna during 1996–2000 we considered a renewal process involving the accumulation and eruption of magma in a shallow reservoir. For vulcanian explosions at Soufrière Hills volcano, however, *Connor et al.* [2003] showed how eruption periodicity is controlled by the competing processes of pressure buildup and gas escape in the upper conduit. In this different scenario, our approach could be modified to consider an alternate eruptive control.

[19] **Acknowledgments.** We thank R. Wright and P. Lundgren for information and discussion regarding the ATSR and InSAR data. Reviews by C. Connor and an anonymous reviewer are greatly appreciated. This is HIGP contribution 1454 and SOEST contribution 6845.

References

Bebbington, M. S., and C. D. Lai (1996), Statistical analysis of New Zealand volcanic occurrence data, *J. Volcanol. Geotherm. Res.*, *74*, 101–110.

Behncke, B., and M. Neri (2003), Cycles and trends in the recent eruptive behavior of Mount Etna (Italy), *Can. J. Earth Sci.*, *40*, 1405–1411.

Berardino, P., G. Fornaro, R. Lanari, and E. Sansosti (2002), A new algorithm for surface deformation monitoring based on small baseline differential SAR interferograms, *IEEE Trans. Geosci. Remote Sens.*, *40*, 2375–2383.

Connor, C. B., and B. E. Hill (1995), Three nonhomogeneous Poisson models for the probability of basaltic volcanism: Application to the Yucca Mountain region, Nevada, *J. Geophys. Res.*, *100*, 10,107–10,125.

Connor, C. B., R. S. J. Sparks, R. M. Mason, C. Bonadonna, and S. R. Young (2003), Exploring links between physical and probabilistic models of volcanic eruptions: The Soufrière Hills Volcano, Montserrat, *Geophys. Res. Lett.*, *30*(13), 1701, doi:10.1029/2003GL017384.

Cronin, S. J., M. Bebbington, and C. D. Lai (2001), A probabilistic assessment of eruption recurrence on Taveuni volcano, Fiji, *Bull. Volcanol.*, *63*, 274–288.

De la Cruz-Reyna, S., and G. Carrasco-Núñez (2002), Probabilistic hazard analysis of Citlaltépetl (Pico de Orizaba) Volcano, eastern Mexican Volcanic Belt, *J. Volcanol. Geotherm. Res.*, *113*, 307–318.

Dvorak, J. J., and D. Dzurisin (1993), Variations in magma supply rate at Kilauea volcano, Hawaii, *J. Geophys. Res.*, *98*, 22,255–22,268.

Dzurisin, D. (2003), A comprehensive approach to monitoring volcano deformation as a window on the eruption cycle, *Rev. Geophys.*, *41*(1), 1001, doi:10.1029/2001RG000107.

Francis, P., and D. A. Rothery (2000), Remote sensing of active volcanoes, *Annu. Rev. of Earth Planet. Sci.*, *28*, 81–106.

Harris, A. J. L., A. L. Butterworth, R. W. Carlton, I. Downey, P. Miller, P. Navarro, and D. A. Rothery (1997), Low-cost volcano surveillance from space: Case studies from Etna, Krafla, Cerro Negro, Fogo, Lascar and Erebus, *Bull. Volcanol.*, *59*, 49–64.

Ho, C.-H. (1996), Volcanic time-trend analysis, *J. Volcanol. Geotherm. Res.*, *74*, 171–177.

Jones, G., D. K. Chester, and F. Shooshtarian (1999), Statistical analysis of the frequency of eruptions at Furnas Volcano, São Miguel, Azores, *J. Volcanol. Geotherm. Res.*, *92*, 31–38.

La Delfa, S., G. Patane, R. Clocchiatti, J.-L. Joron, and J.-C. Tanguy (2001), Activity of Mount Etna preceding the February 1999 fissure eruption: Inferred mechanism from seismological and geochemical data, *J. Volcanol. Geotherm. Res.*, *105*, 121–139.

Lundgren, P., F. Casu, M. Manzo, A. Pepe, P. Berardino, E. Sansosti, and R. Lanari (2004), Gravity and magma induced spreading of Mount Etna volcano revealed by satellite radar interferometry, *Geophys. Res. Lett.*, *31*, L04602, doi:10.1029/2003GL018736.

Mann, D., J. Freymueller, and Z. Lu (2002), Deformation associated with the 1997 eruption of Okmok volcano, Alaska, *J. Geophys. Res.*, *107*(B4), 2072, doi:10.1029/2001JB000163.

Rothery, D. A., M. Coltelli, D. Pirie, M. J. Wooster, and R. Wright (2001), Documenting surface magmatic activity at Mount Etna using ATSR remote sensing, *Bull. Volcanol.*, *63*, 387–397.

Smithsonian Institution (2005), Etna volcano, *Bull. Global Volcanism Network*, *30*(1), 7.

Tilling, R. I., R. L. Christiansen, W. A. Duffield, E. T. Endo, R. T. Holcomb, R. Y. Koyanagi, D. W. Peterson, and J. D. Unger (1987), The 1972–1974 Mauna Ulu eruption, Kilauea volcano: An example of quasi-steady-state magma transfer, *U.S. Geol. Surv. Prof. Pap.*, *1350*, 405–469.

Voight, B. (1988), A method for prediction of volcanic eruptions, *Nature*, *332*, 125–130.

Voight, B., R. P. Hoblitt, A. B. Clarke, A. B. Lockhart, A. D. Miller, L. Lynch, and J. McMahon (1998), Remarkable cyclic ground deformation monitored in real-time on Montserrat, and its use in eruption forecasting, *Geophys. Res. Lett.*, *25*, 3405–3408.

Wright, R., S. Blake, A. J. L. Harris, and D. A. Rothery (2001), A simple explanation for the space-based calculation of lava eruption rates, *Earth Planet. Sci. Lett.*, *192*, 223–233.

B. A. Brooks, Hawaii Institute of Geophysics and Planetology, School of Ocean and Earth Science and Technology, University of Hawaii Manoa, 1680 East-West Road, Honolulu, HI 96822, USA.

L. N. Frazer, Department of Geology and Geophysics, School of Ocean and Earth Science and Technology, University of Hawaii Manoa, 1680 East-West Road, Honolulu, HI 96822, USA.

M. R. Patrick, Department of Geological and Mining Engineering and Sciences, Michigan Technological University, 1400 Townsend Drive, Houghton, MI 49931, USA. (mrp8@cornell.edu)